Controls on the width of tropical precipitation and its contraction under global warming

Aaron Donohoe[1], Alyssa R. Atwood[2,3], Michael P. Byrne[4]

[1]*Applied Physics Lab, University of Washington*

[2]*University of California Berkeley.*

[3]*Georgia Institute of Technology.*

[4]*Imperial College, London.*

Climate models robustly and unanimously predict that the region of intense tropical precipitation will narrow under greenhouse gas forcing. We demonstrate that the meridional width of the annual mean tropical precipitation is nearly identical to the seasonal meridional range of the intertropical convergence zone (ITCZ) and that the contraction of tropical precipitation under greenhouse forcing results from a reduced seasonal range of ITCZ migration. An energetic theory – similar to the often invoked energetic theory for ITCZ shifts based on the hemispheric contrast of energy input to the atmosphere– is developed. The meridional width of tropical precipitation is proportional to the seasonal amplitude of the inter-hemispheric contrast in atmospheric heating divided by the gross moist stability of the tropical atmosphere. Climate models are biased toward overly expansive tropical precipitation resulting from an exaggerated hemispheric contrast of atmospheric heating during solstice seasons. The robust contraction of tropical precipitation under global warming results from increased gross moist stability of the tropical atmosphere mainly due to the rise in tropopause height.

Contractions and expansions of the tropical region have widespread impacts on agricultural productivity, especially in semi-arid regions on the tropical-subtropical borders where water resources are marginal[1]. There is a general consensus in the literature that the arid regions of the Earth have expanded polewards[2,3] over the satellite record. Previous studies have primarily focused on the poleward extent of the arid regions where there is subsiding motion in the Hadley circulation and it is unclear if recent trends result from natural variability or are associated with anthropogenic forcing. Here, we focus on the meridional extent of the intense tropical precipitation – hereafter the width of annual tropical precipitation (WA_{ITCZ})–which is associated with the ascending branch of the Hadley circulation. Previous work has demonstrated that WA_{ITCZ} over the Pacific has contracted in recent decades[4] and robustly contracts in climate models under increased atmospheric CO_2 concentrations[5] although the underlying mechanisms are only beginning to be understood [6].

1 Tropical precipitation width and the seasonal migration of the ITCZ

The ITCZ migrates between 8°N in the boreal summer and 6°S in the austral summer and it has long been realized that the annual mean precipitation is shaped by this seasonal migration[7]; regions within the seasonal march of the ITCZ are moist whereas those outside are dry[8]. Here, we explicitly examine the relationship between the seasonal migration of the ITCZ and WA_{ITCZ} and demonstrate that WA_{ITCZ} is controlled by the seasonal range of the ITCZ migrations in two separate applications:

(1) Double ITCZ bias: The climate model bias toward an overly wide WA_{ITCZ} (the double ITCZ bias) is a consequence of an exaggerated seasonal range of ITCZ migration.

(2) Tropical contraction under global warming: The robust contraction of WA_{ITCZ} under CO_2 forcing results from a decrease in the seasonal range of ITCZ migration.

In general, the annual zonal mean tropical precipitation in CMIP5[9] models is bi-modal with maxima centered around 7° north and south and a weak local minimum near the equator (bottom panel of Fig. 1A). We argue that this bi-modality is simply the time average of a single peaked precipitation lineshape sinusoidally following the insolation with the local minimum occurring in the region where the ITCZ rapidly passes over head[10,11] (near the equator). The local extrema occur in the locations where the ITCZ lingers in vicinity of the edge of the annual range and the width between the modal locations is set by the seasonal range of ITCZ migration.

A common metric of the annual mean ITCZ location is the precipitation centroid (P_{CENT}), defined as the latitude delineating regions of equal area weighted precipitation between 20°S and 20°N[12]. P_{CENT} is preferred over defining the ITCZ as the location of peak precipitation because P_{CENT} accommodates bi-modal precipitation distributions [13] where picking a single peak is problematic and is insensitive to model grids spacing. We expand on this metric by defining two additional quantities relevant to the width of tropical precipitation (see methods for details and Fig. S1A for an illustration): (1) The seasonal range of the ITCZ (SR_{ITCZ}) defined as the centroid of June-July-August (JJA) precipitation minus that in December-January-February (DJF) and (2) The width of annual precipitation (WA_{ITCZ}) defined as the centroid of annual mean precipitation to the

north of P_{CENT} (northern P_{CENT}) minus that defined to the south of P_{CENT} (southern P_{CENT}). In CMIP5 pre-industrial (PI) simulations WA_{ITCZ} varies substantially between 12° and 16° and all but two of the models have larger WA_{ITCZ} than observed (13.4° – Fig. 1B). Model biases in WA_{ITCZ} and SR_{ITCZ} relative to the observations are negligibly impacted by anthropogenic forcing since the PI (Fig. S3). As expected, SR_{ITCZ} and WA_{ITCZ} are strongly (R = 0.91) correlated with a regression coefficient near unity (1.03). In all models the SR_{ITCZ} exceeds the WA_{ITCZ} (values fall below the 1:1 line in Fig. 1B) which is expected since the time average precipitation maxima can not be farther off the equator than the seasonal extremes of ITCZ migration.

The above results indicate that the climate model bias toward a more meridionally expansive and bi-modal tropical precipitation distribution is a consequence of biases toward larger SR_{ITCZ} and we equate this bias with the terminology "double ITCZ". Our definition differs from that in recent literature[14] that equates the double ITCZ bias with the contrast in tropical precipitation between the two hemispheres. We argue that there are two independent modes of tropical precipitation biases: (1) the hemispheric contrast in annual mean tropical precipitation that results from the *annual mean* ITCZ location and (2) the width or degree of bimodality in the tropical precipitation that is governed by the SR_{ITCZ} and is the focus of the current work.

In response to a quadrupling of CO_2, all 17 of the CMIP5 models simulate an intensification of tropical precipitation and a contraction of WA_{ITCZ} (an ensemble average change of 5% change from 14.0° to 13.3°) [5,15,16] characterized by a pinching of the two annual mean tropical precipitation maximums toward the equator (lower panel of Fig. 1A). The reduced WA_{ITCZ} under global

warming results from reduced ITCZ migration off the equator during both the austral and boreal summer (i.e. a reduced SR_{ITCZ} of 5% from 15.4° to 14.6°); upper panel of Fig. 1A). In all climate models, both the WA_{ITCZ} and SR_{ITCZ} decrease under $4XCO_2$ as can be seen from the arrows connecting the PI and $4XCO_2$ values in each climate model pointing down and left. Furthermore, the SR_{ITCZ} reduction under global warming is well correlated (R= 0.89) with the decrease in WA_{ITCZ} across the models with a regression coefficient near unity (1.1), indicating that the amplitude of the contraction of tropical precipitation is governed by how much the SR_{ITCZ} is reduced.

These results collectively demonstrate that the WA_{ITCZ} and its change due to external forcing is tightly linked to the SR_{ITCZ}. In the next section, we develop a theory for SR_{ITCZ} with the aim of understanding both mean state biases and changes under global warming.

2 Mechanisms controlling tropical precipitation width

We begin our discussion of mechanisms controlling the WA_{ITCZ} using an idealized climate model ensemble where we modify the amplitude of the seasonal cycle. In these simulations, the atmosphere is coupled to a slab ocean that covers the entire planet (aquaplanet) and the slab depth is globally uniform but varies between the 5 ensemble members from 2.4 meters to 50 meters. When the ocean is deep, ocean temperatures change little in response to seasonal changes in insolation because most of the insolation changes are transmitted to the surface and stored in the ocean column[17]. As a result, the SST maximum remains near the equator at all times of year, the seasonal ITCZ migration is limited and the annual mean precipitation is singly peaked near

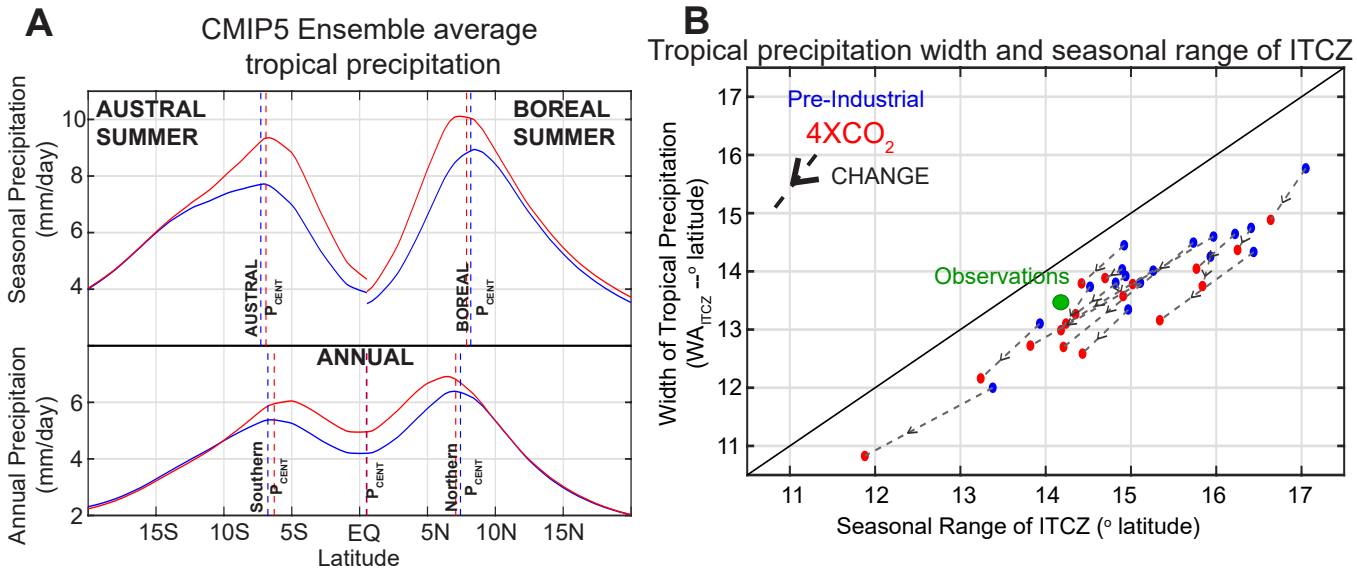

Figure 1: (A) Ensemble and zonal average precipitation in (blue) pre-industrial and (red) 4XCO$_2$ simulations. Austral summer is shown in the upper left, boreal summer in the upper right with vertical lines representing the seasonal ITCZ location (austral/boreal P$_{CENT}$). The annual mean is shown in the bottom panel with vertical dashed lines representing the tropical, Northern and Southern P$_{CENT}$ – see Methods section. (B) Scatter plot of (abscissa) the seasonal range of the ITCZ (SR$_{ITCZ}$) defined from the top panel of A and the (ordinate) annual mean width of precipitation (WA$_{ITCZ}$) defined from the bottom panel of (A). Blue and red dots represent the PI and 4XCO$_2$ values in individual models respectively, and arrows indicate the change. Observational values are shown by the green dot. The black line is the 1:1 line.

the equator (dark blue line in Figure 2A). In simulations with a shallower mixed layer depth, the same seasonal variations in insolation result in much more heating of the surface and adjacent atmosphere such that the temperature maximum and ITCZ migrate off the equator. As a result the annual mean precipitation is smeared across a wider range of latitudes resulting in a bi-modal precipitation distribution. The WA_{ITCZ} increases alongside the SR_{ITCZ} with decreasing ocean depth (Fig. 2A).

An energetic theory for the annual mean ITCZ location has emerged in recent literature[18,19] and, motivated by its success, we extend this theory to analyze SR_{ITCZ}. The starting point for this theory is that the inter-hemispheric atmospheric energy transport and tropical precipitation are both intimately linked to the Hadley cell location; the precipitation is co-located with the ascending branch of the Hadley Cell and the atmospheric energy transport is in the direction of motion in the upper branch of the Hadley cell such that the atmosphere fluxes energy across the equator (AHT_{EQ}) away from the ITCZ with a magnitude proportional to the ITCZ displacement off the equator[20]. Thus, the ITCZ location[14,21,22]and its migration due to external forcing[12] is tightly linked to the AHT_{EQ} demanded by the hemispheric contrast of atmospheric heating.

AHT_{EQ} and ITCZ location are highly ($\mathrm{R}^2 = 0.99$) correlated over the observed (and modeled) climatological seasonal cycle[20]. It has been argued that the annual mean relationship between ITCZ location and AHT_{EQ} is constrained by the climatological seasonal relationship between ITCZ location and AHT_{EQ}[23] since the annual mean ITCZ displacement is a small residual of substantially larger seasonal ITCZ migrations [24]. Here we focus instead on the hemispheric contrast of atmo-

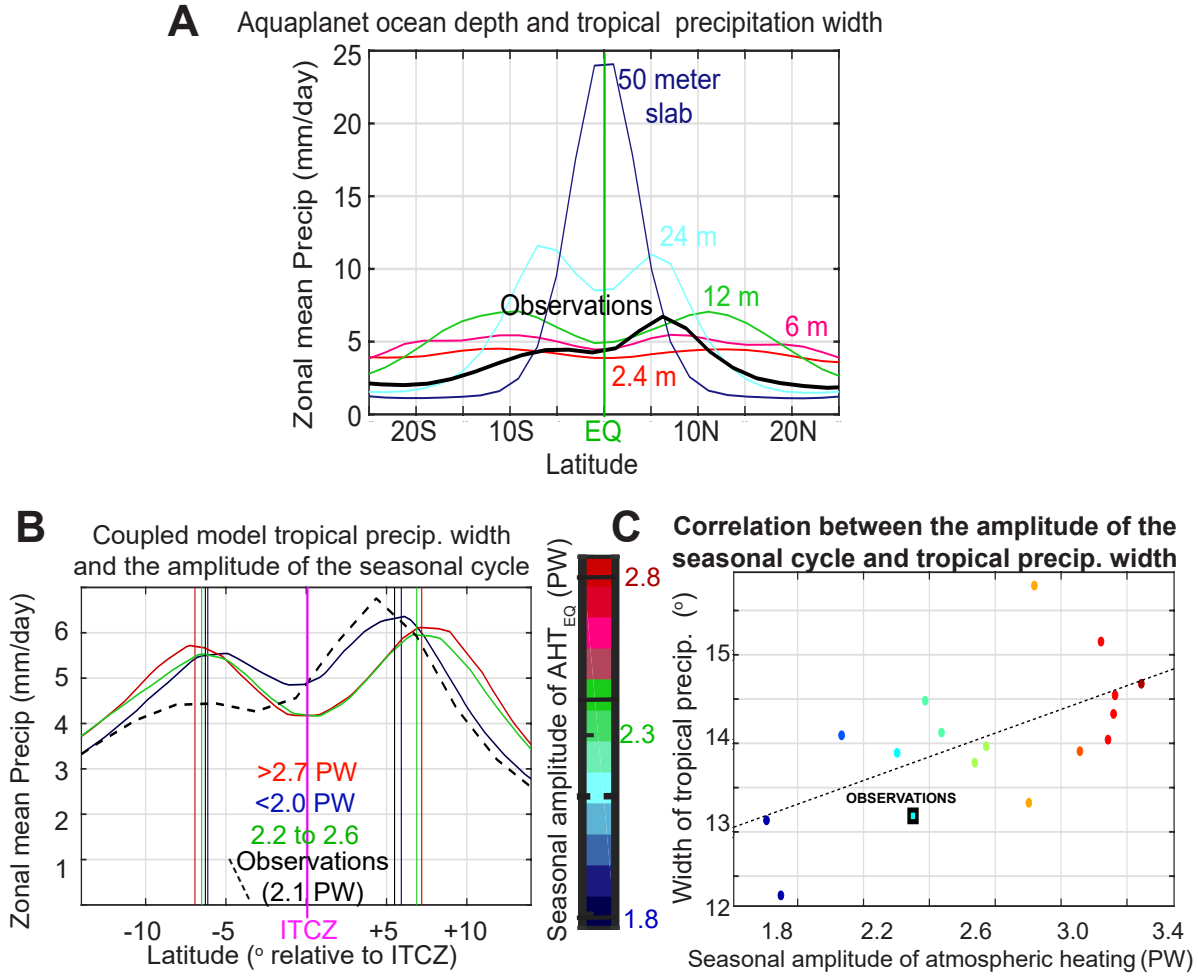

Figure 2: (A) Annual mean precipitation in aquaplanet simulations with varying mixed layer depth. Observed precipitation is shown in black. (B) Zonal mean precipitation in CMIP5 PI models sorted in composites by the magnitude of $\|AHT_{EQ}\|$. The red/green/blue lines are the composite means of precipitation in models with large/intermediate/small amplitude seasonal cycles with $\|AHT_{EQ}\|$ values given in the legend. The observations are shown in the dashed black line and the color coding indicates $\|AHT_{EQ}\|$ as shown in the color bar. Vertical lines show the locations of the NH and SH tropical precipitation centroids used to define the tropical precipitation width. (C) WA_{ITCZ} and $\|AHT_{EQ}\|$ in CMIP5 PI simulations. Observations are shown by the cyan square.

spheric heating/cooling during the solstice seasons, which determine how much the ITCZ must shift off the equator seasonally. The required AHT_{EQ} at any instance is[20]:

$$AHT_{EQ} = \langle SW_{ABS} \rangle + \langle SHF \rangle - \langle OLR \rangle - \langle STOR_{atmos} \rangle \tag{1}$$

where brackets indicate the spatial integral in the SH minus that in the NH, SW_{ABS} is the shortwave absorption in the atmosphere, SHF is the upward flux of latent, sensible and longwave radiation at the surface, OLR is the outgoing longwave radiation and STOR_{atmos} is the energy tendency in the atmospheric column. In the summer hemisphere, the atmosphere is heated from two sources: (1) the direct absorption of solar radiation in the atmospheric column by constituents such as ozone and water vapor and (2) the upward turbulent and longwave radiative energy fluxes from the surface as the ocean and land warm up in response to increased downwelling solar radiation at the surface. These sources of energy to the atmosphere are partly balanced by storage in the column (STOR_{atmos}) and enhanced OLR to space as the column heats up; the remainder of the excess energy is fluxed across the equator (AHT_{EQ}). In the aquaplanet ensemble discussed above, for the deeper ocean simulations, the summer atmosphere is heated primarily by $\langle SW_{ABS} \rangle$ since the sun barely heats the surface to drive upward SHF[17]. In the shallower ocean runs, where the sun can heat the ocean surface, upward turbulent energy fluxes in the summer hemisphere also heat the atmosphere. Thus, the energetics demand a larger magnitude AHT_{EQ} during the solstice seasons in the shallower ocean simulations which results in a larger SR_{ITCZ} and wider WA_{ITCZ}.

From a dynamics perspective, the AHT_{EQ} demanded energetically is accomplished by the

zonal mean mass transport in the Hadley cell (Ψ_{EQ}) acting on the gross moist stability of the atmosphere at the equator (GMS_{EQ}) = $\text{Cp}(\theta_{upper} - \theta_{lower})$ – defined here as the heat capacity (Cp) times the equivalent potential temperature (θ) contrast between the poleward and equatorward flowing air in the upper and lower branches of the Hadley circulation respectively[25,26]:

$$AHT_{EQ} \approx \Psi_{EQ} GMS_{EQ}, \tag{2}$$

where the approximation results from the assumption that eddies do not contribute to AHT_{EQ}. Ψ_{EQ} is proportional to the displacement of the Hadley cell (and thus the ITCZ) off the equator [20] provided the basic structure of the mass overturning streamfunction is maintained. Therefore:

$$SR_{ITCZ} \propto \frac{\|AHT_{EQ}\|}{GMS_{EQ}}, \tag{3}$$

where $\|\|$ brackets denote the amplitude of the annual harmonic (see supporting material for derivation and discussion) and we have assumed that GMS_{EQ} is seasonally (but bot climate state) invariant [27] .

This conceptual framework provides two possible mechanisms for changes and/or inter-model differences in SR_{ITCZ}:

1. Changes in the magnitude of atmospheric heating/cooling during the solstitial seasons: If the atmosphere in the summer hemisphere receives more energy over the summer, the sea-

sonal demand of AHT_{EQ} increases resulting in larger $\|AHT_{EQ}\|$ and SR_{ITCZ} (provided GMS_{EQ} is unchanged). This mechanism accounts for the differences in WA_{ITCZ} across the slab ocean aquaplanet simulations discussed above. Though we have discussed this mechanism in terms of energy input to the summer hemisphere, the relevant metric driving AHT_{EQ} is actually the seasonal amplitude of the hemispheric contrast of energy input to the atmosphere (see Methods).

2. Changes in the gross moist stability of the tropics: In the absence of changes in $\|AHT_{EQ}\|$, an atmosphere with a larger GMS_{EQ} can achieve the same energy transport with a smaller mass overturning circulation at the equator (Ψ_{EQ}) and, thus, a smaller Hadley cell/ITCZ displacement off the equator.

We use this framework to understand the CMIP5 double ITCZ bias and contraction of WA_{ITCZ} under global warming in the next section.

3 Controls on tropical precipitation width in CMIP models

The mechanisms controlling the SR_{ITCZ} discussed in the previous section can be visualized by plotting the seasonal cycles of the AHT_{EQ} and ITCZ location (Fig.3). In this figure, the projection of the line onto the abscissa is equal to $\|AHT_{EQ}\|$, and the slope is the regression coefficient between ITCZ location and AHT_{EQ} ($\propto \frac{1}{GMS_{EQ}}$). Each line is centered on the annual mean AHT_{EQ} and ITCZ location. In the context of the mechanisms discussed above, the SR_{ITCZ} (ordinate range) can differ due to differences in the length of the abscissa (i.e. differences in the seasonal amplitude of atmospheric heating) with fixed slope or, due to differences in the slope (GMS_{EQ}) with fixed

seasonal atmospheric heating.

Cause of double ITCZ biases The inter-model spread of SR_{ITCZ} in PI simulations results primarily (R=0.65) from differences in $\|AHT_{EQ}\|$, whereas the slopes are not significantly correlated with SR_{ITCZ}; the blue lines in Fig. 3 have similar slopes but contrasting lengths (c.f. the fractional ensemble spread of $\|AHT_{EQ}\|$ and slope in the histograms in Fig. 3B,C). This result indicates that the inter-model spread in SR_{ITCZ} results from variations in the seasonal contrast of atmospheric heating and not due to differences in GMS_{EQ}. Since, the SR_{ITCZ} is intricately linked to WA_{ITCZ}, this result is consistent with the finding that inter-model differences in WA_{ITCZ} are primarily (R=0.60) due to differences in the seasonal energy input to the atmosphere (Fig. 2C).

To elaborate on this point, we composite the simulated annual mean precipitation in the PI control runs into three sets based on the value of $\|AHT_{EQ}\|$: (i) large seasonal cycle ($\|AHT_{EQ}\|$ >2.7PW – red line in Fig. 2B), (ii) moderate seasonal cycle (2.2 PW< $\|AHT_{EQ}\|$ <2.6 PW – green line) and (iii) small seasonal cycle ($\|AHT_{EQ}\|$ <2.0 PW – blue line). The tropical precipitation is much more meridionally expansive and has a more pronounced bi-modality in models with a large $\|AHT_{EQ}\|$ as compared to those with a small $\|AHT_{EQ}\|$ (c.f. the red and blue precipitation profiles). The observed $\|AHT_{EQ}\|$ (2.1 PW) is smaller than most of the climate models (black square in Fig. 2C) and the observed meridional profile of tropical precipitation better matches that of the small seasonal cycle composite (c.f. the dashed black line with the dark blue in Fig. 2B) with the added caveat that the hemispheric contrast between tropical precipitation in the NH and SH is larger in the observations than in the models.

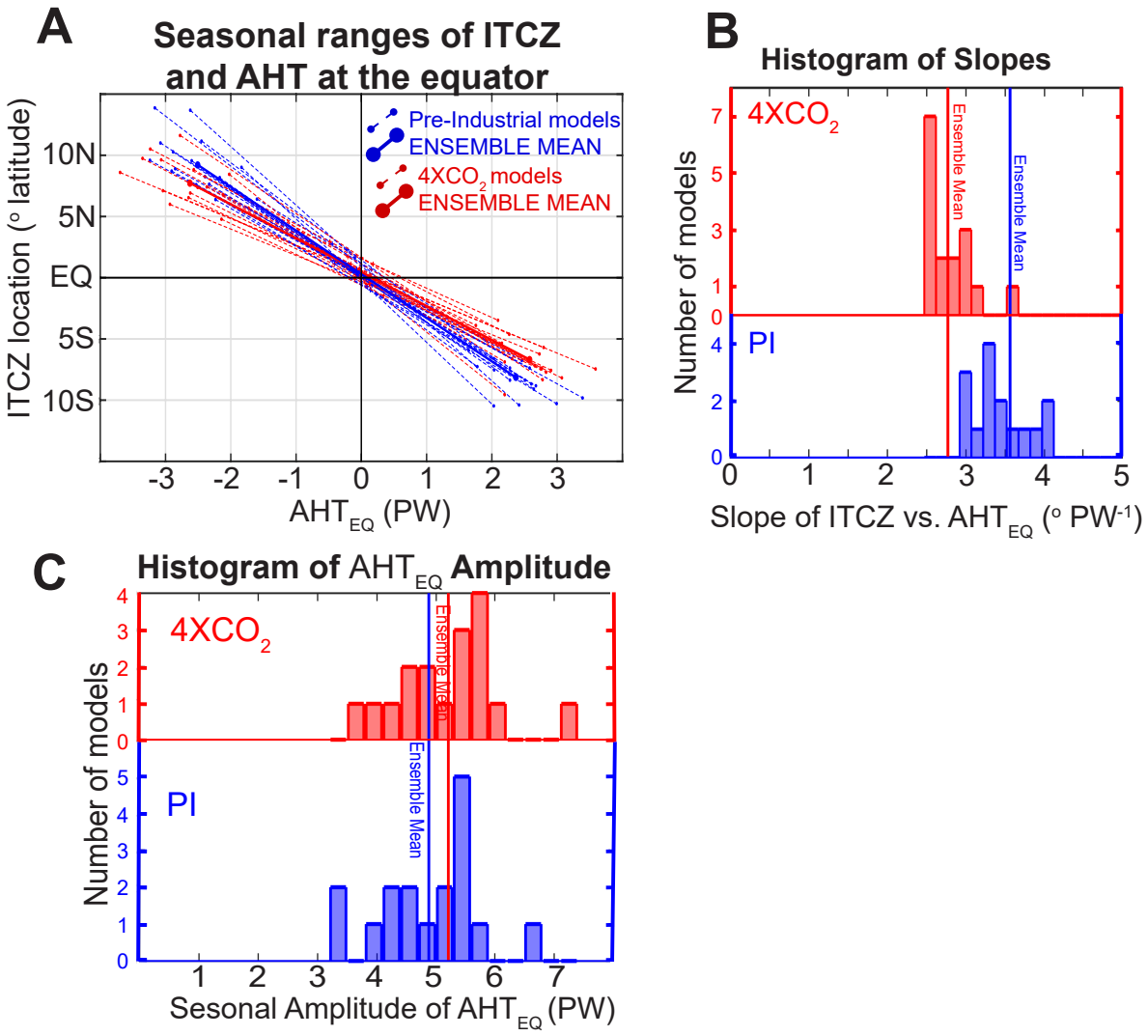

Figure 3: (A) The seasonal relationship between AHT_{EQ} (abscissa) and ITCZ location (ordinate – defined by the precipitation centroid) in CMIP5 PI (blue) and 4XCO_2 (red) simulations. Each line is a different model with the length of the projection onto the abscissa equal to the seasonal amplitude of AHT_{EQ} ($\|AHT_{EQ}\|$) and the slope equal to the regression coefficient between ITCZ location and AHT_{EQ} (see supplemental information for details). Histogram of (B) seasonal slopes and (C) $\|AHT_{EQ}\|$ for PI (blue) and 4XCO_2 simulations.

Cause of tropical precipitation contraction under global warming In response to CO_2 quadrupling, $\|AHT_{EQ}\|$ shows a modest (0.1 PW $\approx$6% of climatology) ensemble average increase – favoring an enhanced SR_{ITCZ}– that is consistent with enhanced absorption of solar radiation in the summer hemisphere due to ice melting and increased absorption by water vapor in the moistened atmosphere[28]. However, counteracting these modest changes in $\|AHT_{EQ}\|$, the seasonal slope between ITCZ location and AHT_{EQ} robustly and unanimously decreases (c.f. the red and blue histograms in Fig. 3B). The ensemble average slope decreases by 22% between PI and $4XCO_2$ from (-3.6 to -2.8° PW^{-1}), favoring a reduced SR_{ITCZ}. As a result of the reduced ITCZ/AHT_{EQ} slope under $4XCO_2$, the SR_{ITCZ} decreases in all models resulting in the contraction of WA_{ITCZ}.

We speculate that the reduced slope between ITCZ location and AHT_{EQ} is a consequence of enhanced GMS of the tropical atmosphere[29,30]. The ensemble average streamfunction during the solstitial seasons (Fig. 4A,B) achieves the slightly larger magnitude AHT_{EQ} (red arrows) energetically required in the $4XCO_2$ simulations, despite having a weaker Ψ_{EQ}. The meridional gradient of the streamfunction is nearly unchanged (not shown) under increased CO_2 suggesting that the net energy input to the tropical atmosphere – which is tied to the atmospheric heat flux divergence and hence the meridional gradient of the streamfunction[19]– is nearly unchanged. As a result, the solstitial Hadley cell in the summer hemisphere shifts equatorward and upward (following the rising tropopause[31]) under global warming relative to its climatological position (c.f. the solid and dashed contours in the upper panels of Fig. 4). The solstitial precipitation maxima (black lines) are co-located with the maximum upward velocities and shift equatorward with the Hadley cell under global warming. The annual average of these robust seasonal results is an equatorward

contraction of the region of heavy precipitation. The fundamental role of changes in the GMS in contracting the tropical precipitation under global warming has been discussed previously[5,6,32] and is supported by our analysis of the relationship between the tropical mass overturning and atmospheric energy transport (see supplemental Fig. S2), which suggests that the equivalent potential temperature contrast between the upper and lower branches of the Hadley cell ($\propto$GMS)[25] increases from 9.7K to 10.8K under 4XCO_2 amounting to a 10% change that more than accounts for the 5% change in SR_{ITCZ}.

4 Discussion

We argue that two distinct types of tropical precipitation biases exist in models that are orthogonal in both their impact on the meridional structure of precipitation and their underlying mechanism: 1. the well-known amplitude contrast of tropical precipitation between the two hemispheres associated with the annual mean ITCZ location [14] that results from the preferential annual mean heating of the NH in the observations[21,22] and 2. the WA_{ITCZ} or meridional distance between the tropical precipitation peaks in the NH and SH – i.e. the double ITCZ – which is intricately connected to SR_{ITCZ} and is governed by the amplitude of seasonal energy input to the atmosphere. Climate models are biased toward amplified hemispheric contrast of seasonal energy input to the atmosphere resulting in overly expansive tropical wet regions. These model biases work in concert with the annual mean energetic arguments previously identified in the literature but it is unclear which is more problematic in accurately representing the mean state of the tropics in climate models; an understanding of the root cause of biases in the seasonal cycle is paramount for future progress in

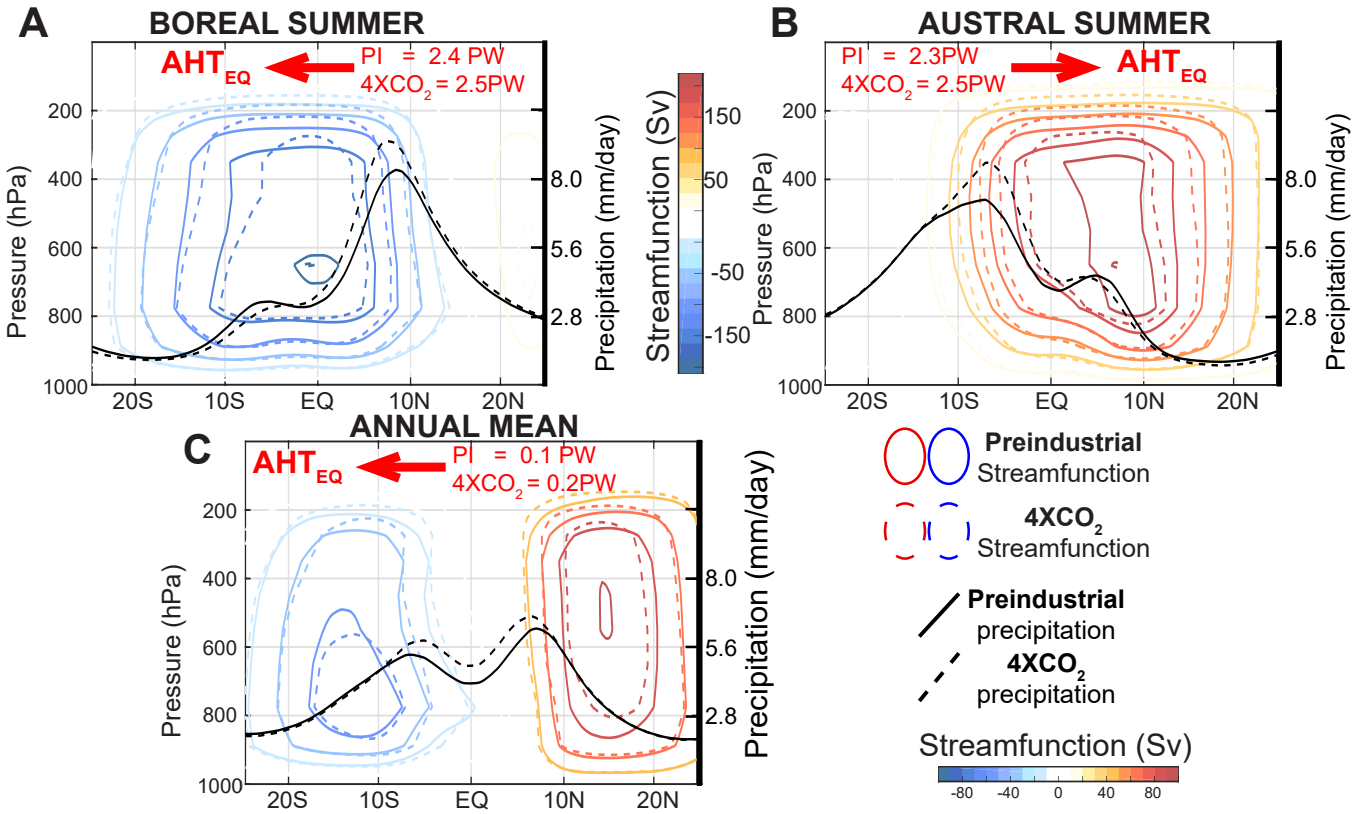

Figure 4: Mass overturning streamfunction (red and blue contours) and precipitation (black lines) for the CMIP5 PI (dashed lines) and $4XCO_2$ (solid lines) ensemble average. The red arrows and numbers show the AHT_{EQ} direction and magnitude. Panel A shows the boreal summer (JA), panel B the austral (JF) summer and panel C the annual mean all with streamfunction contour interval of 30 Sv (1 Sv = 10^9 kg S^{-1}) but with differing magnitude color scaling for the seasonal versus annual plots as shown by the colorbars in the upper and lower panels.

reducing climate model mean state biases.

The robust meridional contraction of tropical precipitation under global warming [15,16] results from enhanced GMS of the tropics. Other studies [5,6,32] have identified changes in GMS as critical to future narrowing of convective zones from annual mean energetic considerations. We offer a complimentary view point that changes in the seasonal range of the ITCZ are an essential ingredient of future tropical precipitation changes. The robust precipitation contraction is in stark contrast to the uncertainty in meridional shifts of the ITCZ under global warming[23] that primarily result from the unknown structure of cloud feedbacks. The mechanism we propose suggests that tropical precipitation should expand meridionally in a cooler climates such as glacial periods and suggests that the implied ITCZ shifts needed to explain hydrological changes deduced from the paleoclimate record[19,33–35] should be reconsidered in light of the contracting mode of tropical precipitation changes.

1. Sivakumar, M., Das, H. & Brunini, O. Impacts of present and future climate variability and change on agriculture and forestry in the arid and semi-arid tropics. *Clim. Chang.* **70**, 31–72 (2005).

2. Johanson, C. & Fu, Q. Hadley cell widening: model simulations versus observations. *J. Climate* **22**, 2713–2725 (2009).

3. Quan, X., Hoerling, M., Perlwitz, J., Diaz, H. & Xu, T. How fast are the tropics expanding? *J. Climate* **27**, 1999–2013 (2014).

4. Wodzicki, K. & Rapp, A. Long term characterization of the pacific itcz using trmm, gpcp, and era-interim. *J. Geophys. Res.* **121**, 3153–3170 (2016).

5. Byrne, M. & Schneider, T. Narrowing of the itcz in a warming climate: Physical mechanisms. *Geophys. Res. Lett.* **43**, 11350–11357 (2016).

6. Byrne, M. & Schneider, T. Energetic constraints on the width of the intertropical convergence zone. *J. Climate* **29**, 4709–4721 (2016).

7. Hadley, G. Concerning the cause of the general tradewinds. *Philos. Trans. Roy. Soc* **29**, 58–62 (1735).

8. Sachs, J. *et al.* Southward movement of the pacific intertropical convergence zone ad 1400-1850. *natgeo* **2**, 519–525 (2009).

9. Taylor, K., Stouffer, R. & Meehl, G. An overview of cmip5 and the experiment design. *Bull. Amer. Meteor. Soc.* **93**, 485–498 (2012).

10. Hu, Y., Li, D. & Liu, J. Abrupt seasonal variation of the itcz and hadley circulation. *Geophys. Res. Lett.* **34** (2007).

11. Xian, P. & Miller, R. Abrupt seasonal migration of the itcz into the summer hemisphere. *J. Atmos. Sci.* **65**, 1678–1695 (2008).

12. Frierson, D. M. W. & Hwang, Y.-T. Extratropical influence on itcz shifts in slab ocean simulations of global warming. *J. Climate* **25**, 720–733 (2012).

13. Bordoni, S. & Schneider, T. Monsoons as eddy-mediated regime transitions of the tropical overturning circulation. *Nature Geosci.* **1** (2008).

14. Hwang, Y. & Frierson, D. Link between the double-intertropical convergence zone problem and cloud bias over southern ocean. *Proc. Nat. Acad. Sci. USA* **110**, 4935–4940 (2013).

15. Lau, W. & Kim, K. Robust hadley circulation changes and increasing global dryness due to co2 warming from cmip5 model projections. *pnas* **122**, 3630–3635 (2015).

16. Su, H. *et al.* Tightening of tropical ascent and high clouds key to precipitation change in a warmer climate. *natcom* (2017).

17. Donohoe, A., Frierson, D. & Battisti, D. The effect of ocean mixed layer depth on climate in slab ocean aquaplanet experiments. *Climate Dyn.* **26**, 15 Pages (2013).

18. Kang, S., Held, I., Frierson, D. & Zhao, M. The response of the itcz to extratropical thermal forcing: idealized slab-ocean experiments with a gcm. *J. Climate* **21**, 3521–3532 (2008).

19. Schneider, T., Bischoff, T. & Haug, G. Migrations and dynamics of the intertropical convergence zone. *nature* **513**, 45–53 (2014).

20. Donohoe, A., Marshall, J., Ferreira, D. & McGee, D. The relationship between itcz location and atmospheric heat transport across the equator: from the seasonal cycle to the last glacial maximum. *J. Climate* **26**, 3597–3618 (2013).

21. Marshall, J., Donohoe, A., Ferreira, D. & McGee, D. The oceans role in setting the mean position of the inter-tropical convergence zone. *Climate Dyn.* 14 (2013).

22. Frierson, D. *et al.* Why does tropical rainfall peak in the northern hemisphere? the role of the oceans meridional overturning circulation. *Nature Geosci.* **6**, 940–944 (2013).

23. Donohoe, A. & Voigt, A. Shifts in the region of tropical precipitation under global warming. In Wang, S., Yoon, J., Gillies, R. & Funk, C. (eds.) *Patterns of Climate Extremes;Trends and Mechanisms* (American Geophysical Union Books, 2015).

24. Chiang, J. & Friedman, A. Extratropical cooling, interhemispheric thermal gradients, and tropical climate change. *Annu. Rev. Earth Planet. Sci.* **40**, 383–412 (2012).

25. Held, I. The partitioning of the poleward energy transport between the tropical ocean and atmosphere. *J. Atmos. Sci.* **58**, 943–948 (2001).

26. Czaja, A. & Marshall, J. The partitioning of poleward heat transport between the atmosphere and the ocean. *J. Atmos. Sci.* **63**, 1498–1511 (2006).

27. Hill, S., Ming, Y. & Held, I. Mechanisms of forced tropical meridional energy flux change. *J. Climate* **28**, 1725–1742 (2015).

28. Donohoe, A., Armour, K., Pendergrass, A. & Battisti, D. Shortwave and longwave contributions to global warming under increasing co_2. *Proc. Nat. Acad. Sci. USA* **111**, 16700–16705 (2014).

29. Chou, C. & Chen, C. Depth of convection and the weakening of tropical circulation in global warming. *J. Climate* **23**, 3019–3030 (2010).

30. Ma, J., Xie, S. & Kosaka, Y. Mechanisms for tropical tropospheric circulation change in response to global warming. *J. Climate* **25**, 2979–2994 (2012).

31. Lorenz, D. & DeWeaver, E. Tropopause height and zonal wind response to global warming in the ipcc scenario integrations. *cd* **112** (2007).

32. Chou, C., Neelin, J., Chen, C. & Tu, J. Evaluating the rich-get-richer mechanism in tropical precipitation change under global warming. *J. Climate* **22**, 1982–2005 (2009).

33. Pahnke, K., Sachs, J. P., Keigwin, L., Timmerman, A. & Xie, S. P. Eastern tropical pacific hydrologic changes during the past 27,000 years from d/h ratios in alkenones. *Paleoceanography* **22** (2007).

34. McGee, D., Donohoe, A., Marshall, J. & ferreira, D. Changes in tropical precipitation, itcz location and hemispheric energy budgets at the last glacial maximum, heinrich stadial 1, and the mid holocene. *Climate of the Past* Submitted. (2013).

35. Arbuszewski, J., deMenocal, P., Clroux, C., Bradtmiller, L. & Mix, A. Meridional shifts of the atlantic intertropical convergence zone since the last glacial maximum. *Nature Geosci.* **6**, 959962 (2013).

36. Xie, P. & Arkin, P. Analyses of global monthly precipitation using gauge observations, satellite estimates, and numerical model predictions. *J. Climate* **9**, 840–858 (1996).

37. Dee, D. *et al.* The era-interim reanalysis: configuration and performance of the data assimilation system. *Quart. J. Roy. Meteor. Soc.* **137**, 553–597 (2011).

38. Kalnay, E. *et al.* The NCEP/NCAR 40-year reanalysis project. *Bull. Amer. Meteor. Soc.* (1996).

39. Delworth, T. L. *et al.* GFDL's CM2 global coupled climate models. part i: Formulation and simulation characteristics. *J. Climate* **19**, 643–674 (2006).

40. Held, I. & Soden, B. Robust responses of the hydrological cycle to global warming. *J. Appl. Meteor.* **19**, 5686–5699 (2006).

41. Donohoe, A., Marshall, J., Ferreira, D., Armour, K. & McGee, D. The inter-annual variability of tropical precipitation and inter-hemispheric energy transport. *J. Climate* **27**, 3377–3392 (2013).

Acknowledgments AD and ARA were funded by the National Science Foundation Paleo Perspective on Climate Change (P2C2) Grant number AGS-1702827.

Author contributions AD, ARA and MPB contributed to the conceptual and theoretical development of the ideas presented here. AD performe the observational and model analysis. competing financial interests.

Competing Interests The authors declare that they have no competing financial interests.

Correspondence Correspondence and requests for materials should be addressed to A.D. (email: adonohoe@u.washington.edu).

Methods

Data-sets and model simulations used Observational precipitation estimates are taken from the National Oceanographic and Atmospheric Administration (NOAA) Climate Prediction Center (CPC) merged analysis[36] climatology defined from 1981 to 2016. Observational-based mass overturning streamfunctions and MSE are derived from ERA interim[37] and NCEP[38] atmospheric winds, temperature, geopotential height and specific humidity. An average of NCEP and ERA based climatologies is computed over the 1981-2016 time period. Streamfunctions are defined from the pressure integral of the zonally integrated meridional velocity after a barotropic wind correction to ensure zero mass flux through a latitudinal circle is applied.

Pre-industrial (PI) and abrupt carbon dioxide quadrupling ($4XCO_2$) simulations from 17 coupled climate models participating in the Coupled Model Inter-comparison Project Phase 5 (CMIP5)[9] are analyzed. We use all models that make publicly available the required output fields of precipitation, top-of-atmosphere radiation, radiative and turbulent energy fluxes at the surface and three dimensional atmospheric winds, temperature, geopotential height and specific humidity. Atmospheric energy transport was calculated from the residual of TOA radiation, surface energy fluxes and atmospheric column-integrated energy tendency[20]. PI climatologies were composed from the last 50 years of simulations and $4XCO_2$ climatologies were composed from 50-100 years after instantaneous CO_2 quadrupling.

We note that our assessment of model biases by comparing PI simulations to the 1981-2016 observational period may be impacted by the climate response the anthropogenic forcing since the

PI. We diagnose the magnitude of tropical precipitation differences between the PI and historical observation period in the climate models where historical simulations are available (Fig. S3). The differences in both the SR_{ITCZ} and the WA_{ITCZ} between the PI and historical period are small in all models (c.f. the blue and black dots connected by black lines) compared to both the ensemble mean bias relative to the observations and the magnitude of the change due to $4XCO_2$ (Fig. 1B). Importantly, the model bias in the width of tropical precipitation identified in the PI ensemble is similar to that in the historical simulations over the observational period and is negligibly affected by anthropogenic forcing between the PI and historical period.

The ensemble of aquaplanet simulations with different slab-ocean depths are fully described in Donohoe et al. 2013[17]. In short, these simulations couple the GFDL 2.1 atmospheric model[39] to a slab ocean with globally uniform depth varying from 2.4m to 50m (5 different ensemble members). The insolation varies seasonally with modern-day obliquity (23.439°) and zero eccentricity.

Data availability: All CMIP5 data are available from the World Climate Research Program's (WCRP) Program For Climate Model Diagnosis and Intercomparison (PCMDI) data access portal (`https://cmip.llnl.gov/cmip5/data_portal.html`). Obsevational precipiation data are available from the NOAA CPC) website (`https://www.esrl.noaa.gov/psd/data/gridded/data.cmap.html`). Observational reanalysis data used to calculate the atmospheric energy fluxes are available from the following sources: (1) NCEP reanalysis are saved on the NOAA Earth System Research Laboratory (ESRL) website (`https://www.esrl.noaa.gov/psd/data/gridded/data.ncep.reanalysis.html`); (2) ERA reanalysis are available on the European Centre for Medium-Range Weather Forecasts (ECMWF) data portal

(http://apps.ecmwf.int/datasets/).

Definition of the seasonal range of ITCZ (SR_{ITCZ}) and width of annual tropical precipitation (WA_{ITCZ}) We define the width of the annual mean tropical precipitation as the meridional separation between the local precipitation maxima in the NH and SH tropics using the following definitions:

Annual-mean ITCZ location: we mark the annual mean ITCZ location as the precipitation centroid (P_{CENT}) defined as the latitude delineating regions of equal magnitude spatially weighted precipitation between 20S and 20N as has commonly been used in the literature[12,20].

Northern P_{CENT} and Southern P_{CENT}: these quantities are intended to capture the location of the tropical precipitation maxima in each hemisphere and are defined as the latitude demarcating regions of equal magnitude spatially weighted precipitation between the annual-mean P_{CENT} (above) and 15° poleward of P_{CENT}

The width of annual mean precipitation: defined as the Northern P_{CENT} minus the Southern P_{CENT} as shown by the purple bar in the lower panel of Fig S1A.

The seasonal range of the ITCZ is defined as the difference in the latitude of ITCZ location during boreal summer (defined as July and August average – JA) minus that in austral summer (January and February – JF) as follows (green bar in Fig S1A): for each season, we iteratively search for the latitude that demarcates regions of equal area weighted precipitation within a 30° wide region – hereafter the boreal and austral P_{CENT}. For example, to define the boreal P_{CENT},

we first define the latitude that demarcates areas of equal JA area weighted precipitation between 15°S and 15°N. In the second iteration, we search for the latitude that demarcates regions of equal precipitation between 15° north and south of the solution from the first iteration. We repeat this procedure until the solution converges (10 iterations). This procedure gives a boreal and austral P_{CENT} that is near the latitude of maximum precipitation (c.f. the vertical dashed blue lines with the peak in the precipitation shown by the solid blue curve in the upper panel of Fig. S1A). We elect to use this iterative definition of the ITCZ in place of the more traditional P_{CENT} defined between fixed latitudes of 20°S and 20°N used elsewhere in the literature[12,19,20] because the latter definition of the ITCZ location and its change due to external forcing is sensitive to changes in precipitation in the region of subsidence in the winter hemisphere, far from the convective precipitation. Specifically, under global warming the precipitation increases in the region of intense precipitation and decreases in the region subsidence[40], with the former effect pushing the traditional P_{CENT} poleward and the latter pulling the P_{CENT} equatorward with a net effect near zero. We wish to highlight changes in the location of peak precipitation only without the complicating effects of changes in the region of descending motion.

The meridional heat transport in the atmosphere is calculated as follows[20,21,41]:

(1) The observational heat transport is calculated as the vertical and zonal integrated moist static energy flux across a latitude band from the 6-hourly reanalysis fields after applying a mass flux correction. The average of ERA interim[37] and NCEP [38] climatologies from 1981-2016 is reported.

(2) In model simulations, the atmospheric energy transport divergence is calculated as that required

to balance the atmospheric energy budget from the residual of the top-of-atmosphere radiation, surface energy flux minus the atmospheric column-integrated energy tendency. The atmospheric heat transport at each latitude is then calculated as the spatial integral of the atmospheric heat flux divergence over the polar cap bounded by the latitude after first applying a spatially invariant adjustment to ensure the global mean atmospheric heat flux divergence is zero – so that the meridional atmospheric heat transport is equal to zero at both poles. The column energy tendency is calculated as the centered finite difference of the vertical mass integral of $C_P T + Lq$ where C_P is the heat capacity of air at constant pressure, T is the atmospheric temperature, L is the latent heat of vaporization of water and q in the specific humidity.

The seasonal amplitude of AHT_{EQ} ($\|AHT_{EQ}\|$) is defined as the amplitude of the annual harmonic in AHT_{EQ}. The seasonal cycle of ITCZ location and AHT_{EQ} are very strongly anti-correlated (R = -0.99) in the observations and on in coupled model simulations (R = -0.91). For this reason, the product of the seasonal relationship between ITCZ location and AHT_{EQ} – defined as the linear regression over the climatological seasonal cycle– and the seasonal amplitude of AHT_{EQ} accurately determines the SR_{ITCZ} (R^2 = 0.96) [20].

Derivation of Eq. 3 and discussion of limitations We seek an expression for the changes in AHT_{EQ} over the seasonal cycle, using Eq. 2 as a starting point. We begin with two assumptions; (1) energy transport across the equator by atmospheric eddies is small in magnitude compared to that by the Hadley circulation – as supported by Fig. S4 and (2) seasonal variations in GMS_{EQ} (denoted by primes) expressed as a fraction of the annual mean GMS_{EQ} (denoted by $\overline{overbars}$) are small compared to those in Ψ_{EQ} ($\left|GMS'_{EQ}/\overline{GMS_{EQ}}\right| << \left|\Psi'_{EQ}/\overline{\Psi_{EQ}}\right|$) – as supported by

the tight correlation between AHT_{EQ} and Ψ_{EQ} shown in Fig. 5A of Donohoe et al. [20]. If the Hadley cell was translated meridionally (d ITCZ_{shift}) alongside the precipitation distribution with no change in the underlying mass overturning streamfunction structure, the resultant change in AHT_{EQ} would be:

$$\frac{dAHT_{EQ}}{dITCZ_{shift}} \approx \frac{d\Psi}{d\theta} GMS_{EQ}. \tag{4}$$

Applying the seasonal magnitude operator (annual harmonic) to Eq. S4 and rearranging gives:

$$SR_{ITCZ} \approx \frac{1}{d\Psi/d\theta} \left[\frac{\|AHT_{EQ}\|}{GMS_{EQ}} - \frac{\overline{AHT_{EQ}}}{\overline{GMS_{EQ}}^2} \left\| \overline{GMS_{EQ}} \right\| \right]. \tag{5}$$

The first term is associated with seasonal variations in the AHT_{EQ} and the second term is associated with seasonal variations in GMS_{EQ}. The second term is negligible when $\|GMS_{EQ}\| \,/\, \left|\overline{GMS_{EQ}}\right| << \|AHT_{EQ}\| \,/\, \left|\overline{AHT_{EQ}}\right|$. $\|AHT_{EQ}\| \,/\, \left|\overline{AHT_{EQ}}\right| \approx 20$ in PI CMIP5 models whereas $\|GMS_{EQ}\| \,/\, \left|\overline{GMS_{EQ}}\right| \approx 0.2$ – the seasonal variations in AHT_{EQ} are an order of magnitude bigger than the annual mean whereas those in GMS_{EQ} are an order of magnitude smaller. As a result, we can neglect the second term to derive Eq. 3 of the manuscript with the constant of proportionality of $\frac{1}{d\Psi/d\theta}$. We have assumed above that: (1) the ITCZ migrates alongside the Hadley cell and (2) the underlying spatial structure of the Hadley cell streamfunction in maintained. In the observed seasonal cycle, the Hadley cell streamfunction does evolve seasonally with the winter cell intensifying while the summer cell nearly vanishes [24] and the ITCZ is located within the winter cell [20] – moving less than the streamfunction zero. However, noting that the Boreal and Austral summer circulations are nearly anti-symmetric about the equator, we could instead linearize Eq. S4 about the solstitial seasons to

consider how far solstitial season ITCZ would have to move to satisfy energetic constraints.

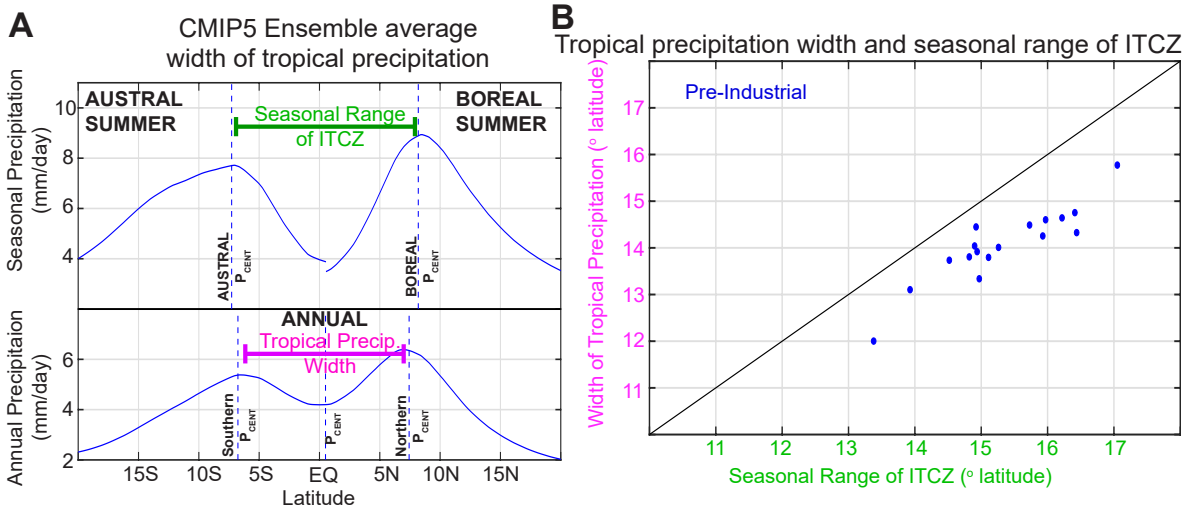

Figure S.1: Demonstration of the definitions of seasonal range of ITCZ (SR_{ITCZ}) and width of annual tropical precipitation (WA_{ITCZ}). (A) CMIP5 PI ensemble and zonal average precipitation. Austral summer is shown on the upper left and boreal summer in the upper right with vertical dashed lines representing the seasonal ITCZ location (austral/boreal P_{CENT}). SR_{ITCZ} is defined as the difference between the boreal P_{CENT} and austral P_{CENT} shown by the green bar. The annual mean precipitation is shown in the bottom panel with vertical dashed lines representing the tropical, Northern and Southern P_{CENT} – see Methods section. WA_{ITCZ} is defined as the difference between Northern P_{CENT} and the Southern P_{CENT} as shown by the purple bar. (B) Scatter plot of (abscissa) the SR_{ITCZ} and the (ordinate) WA_{ITCZ} for each CMIP5 PI simulation. The black line is the 1:1 line.

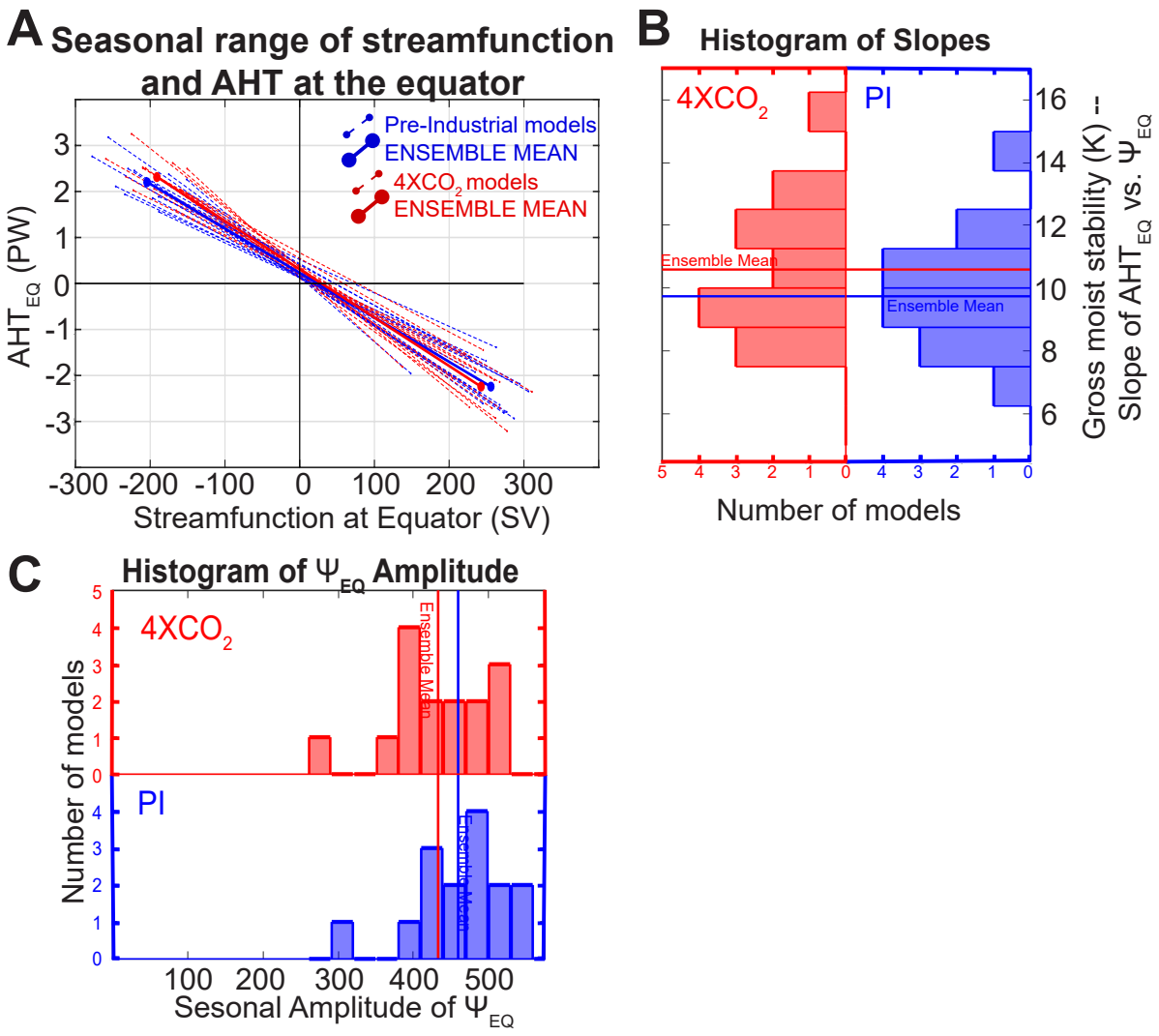

Figure S.2: (A) The seasonal relationship between streamfunction magnitude, Ψ_{EQ} (at the altitude of maximum absolute value – ordinate) and AHT_{EQ} (abscissa) in CMIP5 PI (blue) and 4XCO$_2$ (red) simulations. Each line is a different model with the length of the projection onto the abscissa equal to the seasonal amplitude (annual harmonic) of Ψ_{EQ} and the slope equal to the regression coefficient. (B) Histogram of seasonal slopes converted into the gross moist stability in units of the moist potential temperature (mass flux weighted) contrast between air in the poleward and equatotward branches of the mass overturning circulation.(C) Histogram of the seasonal amplitude of Ψ_{EQ} for PI (blue) and 4XCO$_2$ simulations. The solid red and blue lines in the histograms show the ensemble average of the PI and 4XCO$_2$ simulations respectively.

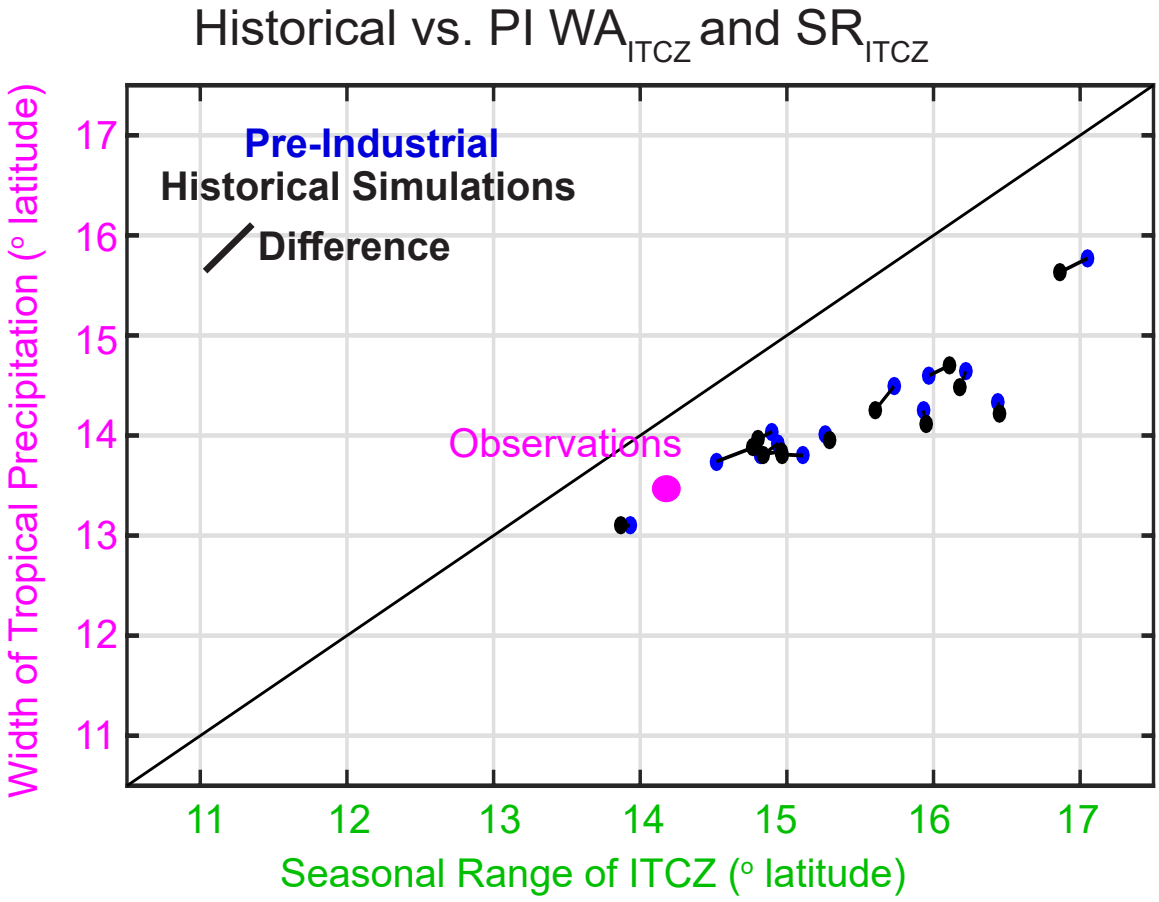

Figure S.3: **Comparison on tropical precipitation width between PI and historical simulations:** Scatter plot of (abscissa) the SR_{ITCZ} and the (ordinate) WA_{ITCZ} for each CMIP5 simulation. The blue dots are the PI simulations and the black dots are the 1981-2016 average of the historical simulations with the black lines connecting results in the same climate model. The averaging dates were chosen to match the observational period shown by the purple dot. The black line is the 1:1 line.

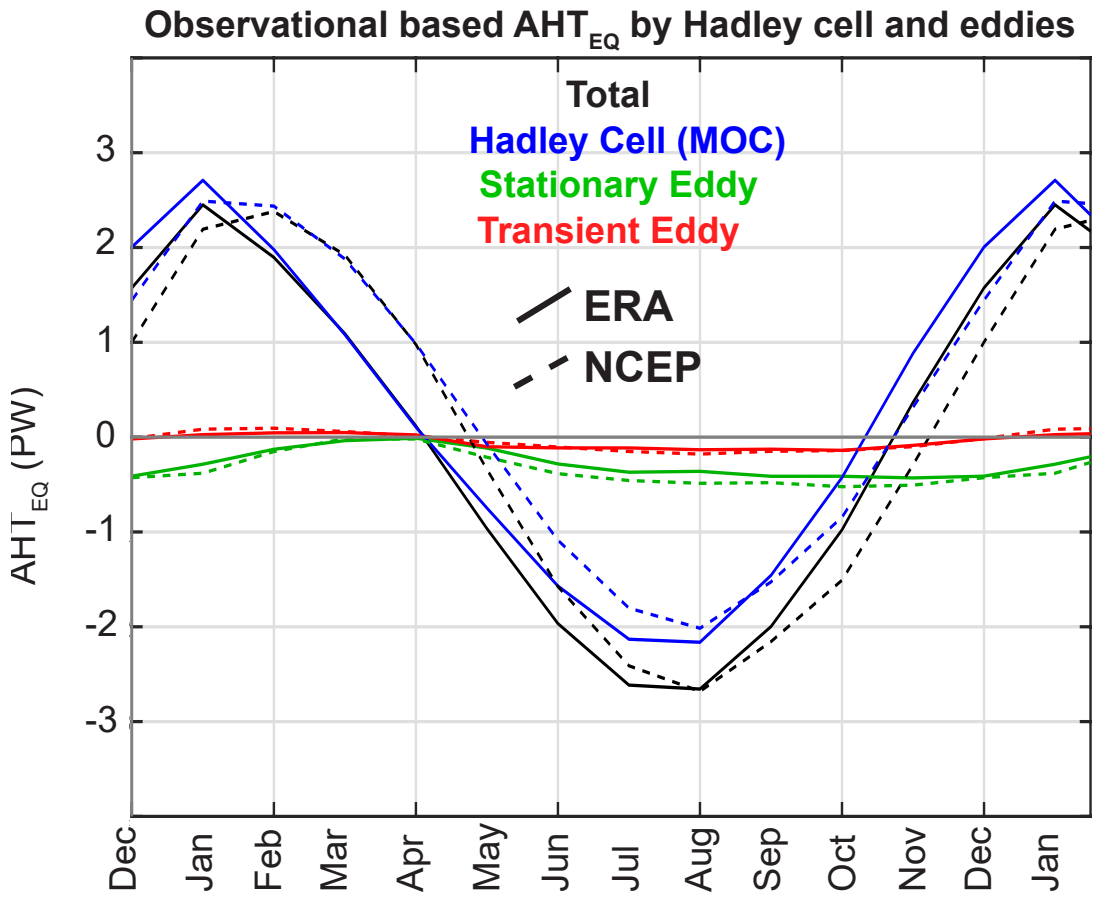

Figure S.4: Observational based seasonal cycle of atmospheric heat transport across the equator (total in black) partitioned into Hadley cell overturning (MOC– blue), stationary eddied (green) and, transient eddies (red). The dashed lines are estimates from the NCEP reanalysis and the solid lines are estimates from ERA reanalysis.